Continuous Visual Navigation with Ant-Inspired Memories

Gabriel Gattaux, Antoine Wystrach, Julien R Serres, Franck Ruffier

Continuous Visual Navigation with Ant-Inspired Memories

Gabriel Gattaux

gabriel.gattaux@univ-amu.fr

Aix-Marseille University - Institute of Movement Science https://orcid.org/0000-0002-9424-7543

Antoine Wystrach

CNRS - Université Paul Sabatier https://orcid.org/0000-0002-3273-7483

Julien Serres

Aix Marseille University https://orcid.org/0000-0002-2840-7932

Franck Ruffier

Aix-Marseille Univ, CNRS https://orcid.org/0000-0002-7854-1275

Article

Keywords:

Posted Date: December 5th, 2024

DOI: https://doi.org/10.21203/rs.3.rs-5505975/v1

Additional Declarations: There is **NO** Competing Interest.

Continuous Visual Navigation with Ant-Inspired Memories

Gabriel Gattaux[1*], Antoine Wystrach[2], Julien R. Serres[1,3], Franck Ruffier[1]

[1*]Aix Marseille Univ, CNRS, ISM, Marseille, France.
[2]Univ Toulouse, CRCA, CBI, UMR CNRS-UPS 5169, Toulouse, France.
[3]Institut Universitaire de France, IUF, Paris, France.

*Corresponding author(s). E-mail(s): gabriel.gattaux@univ-amu.fr;

Abstract

Solitary foraging ants excel in following long visual routes in complex environments with limited sensory and neural resources—an ability that remains challenging for robots with minimal computational power. Here, we introduce a self-supervised, insect-inspired neural network that enables robust route-following on the compact, low-cost Antcar robot. The robot leverages key aspects of ant brain and behavior: (i) continuous, one-shot visual route learning using panoramic encoding in a mushroom body-inspired network, (ii) categorization of low-resolution egocentric panoramas via oscillatory movements, (iii) opponent-process control of angular and forward velocities based on visual familiarity, (iv) recognition of places of interest along routes, and (v) motivation-based memory modulation. Antcar autonomously followed routes between indoor or outdoor destinations, forward or backward, while remaining stable in both theoretical analysis and real-world testing despite occlusions and visual changes. Across 1.3 km of autonomous travel, Antcar achieved challenging route-following with sub-20 cm lateral error at speeds up to 150 cm/s, requiring only 148 kilobits of memory and processing panoramas every 62 ms. This efficient, brain-inspired architecture stands out from more sensor-intensive and computationally demanding methods, presenting a neuromorphic approach with valuable insights into insect navigation and practical robotic applications.

Introduction

Insect navigation has long intrigued researchers across various fields, from biology to robotics, driving the development of cutting-edge technologies for autonomous mobile robots [1–3]. Autonomous navigation remains a demanding and interdisciplinary challenge with applications ranging from space exploration to last miles delivery [4, 5], especially in scenarios where robots cannot rely on satellite systems [6]. Simultaneously, robots serve as valuable tools for studying insects navigation and brain structure, advancing neuromorphic engineering [7–11].

In Robotics, visual teach-and-repeat methods combined with dead-reckoning techniques have gained in popularity [12–15]. However, experienced solitary foraging ants navigate along familiar routes using only visual memories, without relying on dead reckoning (so-called path integration in the insect literature) [16–18]. This behavior has inspired various robotic models, although current implementations are generally limited to short-range experiments of about ten meters, with modest computational efficiency, precision, and accuracy [19–23]. While ant-inspired models achieve results comparable to conventional computer vision approaches [13, 24], they struggle in dynamic environments where computational efficiency must be balanced with resource use.

Fig. 1 Biological inspiration for robotic navigation. An ant in the foreground symbolizes nature's efficient navigational strategies, while the Antcar robot in the background integrates these principles into a neuromorphic system. The blurred image captures only the large masses of the environment, similar to the low-pass spatial filter in the ant's visual system, which retains these large features even when objects obstruct the view between the robot and the building. ©Tifenn Ripoll - VOST Collectif / Institut Carnot STAR.

These challenges are partly due to early navigation models that emphasized hymenopteran behavior rather than underlying brain processes. Early models, referred to as perfect memory models, stored periodic snapshots at specific waypoints [25, 26]. Then, during autonomous route following (or exploitation), forced scanning movements compared acquired views to an image bank, using

rotational image differences to establish the most familiar image and desired heading –a process known as the visual compass [27–32]. However, these approaches has revealed two main limitations when applied in robotics.

The first limitation involves the cumulative storage of snapshots, which significantly increases memory and computational demands as the route lengthens, making it unsuitable for long-distance navigation. This issue was partially addressed by a neural network using the *Infomax* algorithm [33], which enables efficient encoding of increasing numbers of images without a corresponding rise in memory load [20, 31, 34]. However, *Infomax* requires substantial adjustments to synaptic weights for each input through a non-local learning mechanism, limiting its biological plausibility.

In parallel, research on the Mushroom Body (MB), a key part of the insect brain, has highlighted its essential role in olfactory and visual learning [35, 36]. In the MB, learning occurs through synaptic depression between thousands of Kenyon Cells (KCs) – intrinsic neurons that sparsely encode sensory input – and a few Mushroom Body Output Neurons (MBONs), which modulate behavioral responses based on learned associations. These processed signals are then transmitted to downstream neural circuits, influencing decision-making [37]. The first MB model simulating visual route following used a Spiking Neural Network with 20,000 KCs and one MBON to compute familiarity [38]. Despite this advancement, a second limitation remains: a forced systematic scanning during navigation slows robotic movement [21]. Also, this limitation does not reflect natural ant behavior, where scanning occurs only occasionally [39–41].

To address the second limitation, an early robotic implementation combined a *klinokinesis* model with perfect memory, enhancing short-distance route-following by replacing cumbersome scanning with alternating, ballistic left and right turns where familiarity adjusted turn amplitude [19] (later also observed in ants [42]).

To move beyond the random, undirected movement of kinesis, a taxis model was proposed, simulating directed movement toward a stimulus. In this model, KC firing activity was categorized into two distinct MBONs based on left or right orientation relative to the goal [43, 44]. This approach mirrors how insects, through continuous lateral body oscillations, sample multiple directions based on their nest position [42, 45]. Subsequent robotic models for route following attempted to integrate this lateralized approach by splitting the visual field into separate left and right memories, but these implementations showed limited efficiency in real-world tasks [22, 46]. In ants, however, the entire field of view is sent to the MB, and memories are fundamentally binocular [47].

Here, we propose the lateralized route memories model, an MB-inspired design with four MBONs: two dedicated to route following and two for recognizing route extremities (Fig. 2). During a one-shot outbound learning route, ant-like body oscillations are simulated through continuous in-silico rotation of the panoramic image, mimicking head movement. This simulated head orientation, relative to the dynamic local orientation of the route, categorizes views into left or right memory based on the polarity of the angular value, leading to a self-supervised model for route learning. This design also mimics dopaminergic feedback from motor centers, modulating MBON synapses based on the currently active KCs and the integration of left and right stimuli [44].

In addition, our model incorporates key aspects of ant navigation not previously applied in MB models, such as adjusting forward speed by accelerating on familiar routes and slowing down in unfamiliar areas [39]. Our model also enables bi-directional route learning, allowing to retrace a route while moving backward or forward, recognizing visual memories from the outbound journey [48–51]. Embedded in the compact Antcar robot (Figs. 1 and 2a), the model was tested across 99 autonomous trajectories, covering 1.3 km indoors and outdoors, achieving median lateral and angular errors of 20 cm and 3°, respectively, with refresh rates of 16 Hz during exploitation and 38 Hz during learning. Our MB model showed strong robustness to visual changes, including light fluctuations and pedestrian interference. This performance demonstrates the potential of our MB model for efficient, adaptable visual navigation in complex environments with accessible hardware and minimal computing requirements.

Results

Our proposed MB model emulates ant visual processing by encoding panoramic images as ultra-low resolution neural representations, enabling efficient learning and route recognition with minimal computational demands (see Methods for details, Fig. 2b). The model operates in two main phases: learning (Fig. 2c) and exploitation (Fig. 2d). During the learning phase, our self-supervised model encodes the route using two MBONs and stores place-specific memories for the Nest and Feeder as route extremities (see Methods, Fig. 2c). In the exploitation phase, the robot processes each view through both memory pathways, yielding two familiarity values (left and right MBON activities). The lateralized difference of familiarities (λ_{diff}) directs steering, while the maximum familiarity value modulates forward speed. Additionally, a motivational control modulates motor gain, allowing the robot to stop or reverse based on a familiarity thresholds set by place-specific MBONs (see Methods, Fig. 2d).

This study begins with an offline analysis of the proposed self-supervised MB model using two route MBONs to assess stability, followed by experimental route-following tasks in challenging indoor and outdoor environments. Next, a homing task is described, in which the robot follows a long outdoor route in reverse toward the starting area, designated as the Nest (N), and stops nearby, utilizing three MBONs. Finally, a shuttling task is introduced, where the robot, after a single learning trial with two route MBONs and two extremities MBONs for the Nest and Feeder, autonomously shuttles *to and fro* between these two locations, driving both forward and backward.

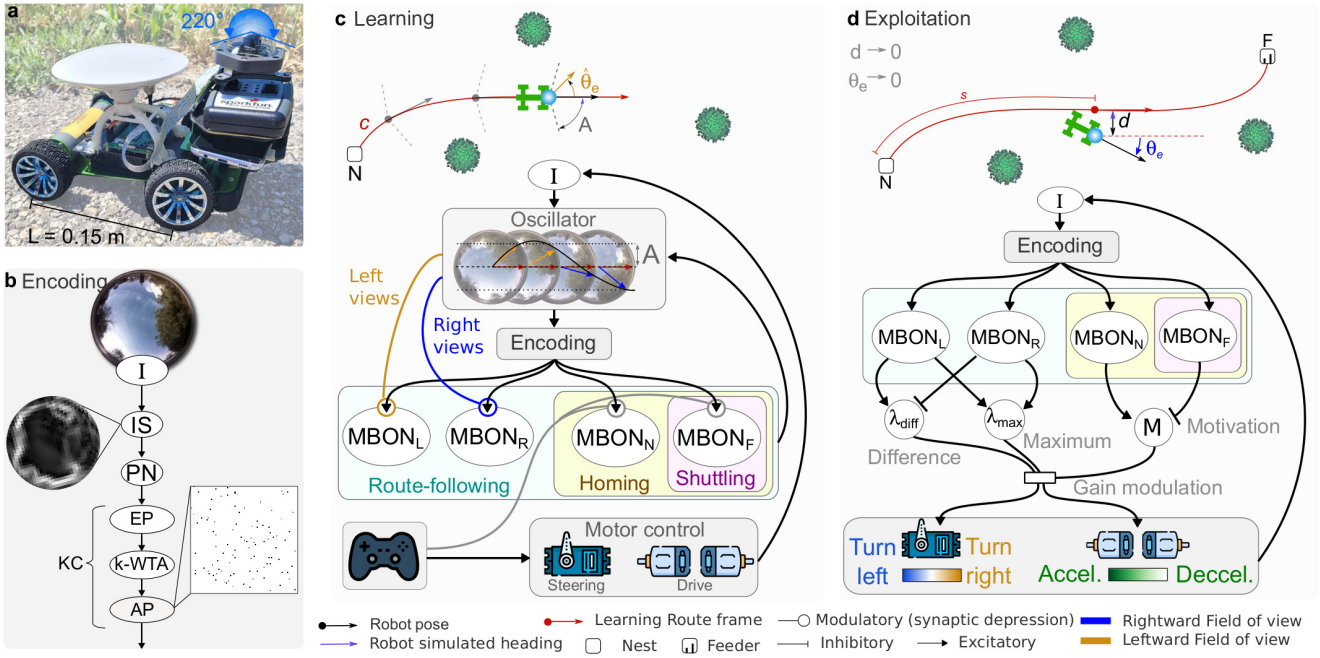

Fig. 2 Overview of the Lateralized Route Memories model implemented in the Antcar robot. This figure illustrates the process from image encoding to navigation control in both learning and exploitation phases. **a** The Antcar robot: a compact car-like platform equipped with an omnidirectional camera and a (Global Positioning System - Real-Time Kinematic) GPS-RTK system for ground truth data. **b** The image encoding process mimics ant's visual processing. Panoramic images (I) are captured, blurred, subsampled, and edge-filtered to create a low-resolution 32×32 pixels panorama (IS). The IS is then transformed into Projection Neurons (PN), which are expanded into Excitatory Post-Synaptic Projections (EP) and reduced into Action Potentials (AP) via a κ-WTA function, forming the Kenyon Cells (KC). **c** During learning, the robot follows a path (C) from a start point (N) with an oscillatory movement to simulate angular deviations ($\hat{\theta_e}$). Synaptic updates occur in the Mushroom Body Output Neurons (MBONs) through the modulation by Dopaminergic-like Neurons (DAN), associating visual inputs with route memories in a self-supervised manner, dependent on the sign of θ_e. An internal oscillator adjusts the image to simulate different angular errors, while joystick inputs control learning dynamics. **d** During exploitation, the robot aims to minimize the lateral (d) and angular (θ_e) errors relative to the route. The encoded image activates the MBONs according to the learned synaptic weights, allowing the robot to determine the position of the route and adjust its steering angle and speed. Familiarity indexes (λ) of MBONs work in an opponent valence process to guide navigation: steering adjustments are based on differentiated familiarities, while the maximum familiarity modulates the speed. Specific MBONs related to start and end points alter motivational states to adjust route polarity or stop movement.

Self-supervised lateralized route memories model

We first evaluated the self-supervised model for route learning (using only two MBONs) with a dataset of indoor and outdoor parallel routes (Figs. 3c,f). Results demonstrated that, with a controlled oscillation amplitude during learning, the model accurately estimated its heading error based on the differential familiarity λ_{diff}, handling angular deviations up to 135° indoors and 90° outdoors (Fig. 3a,d,g). Furthermore, the maximum familiarity index λ_{max}, used as feedback for speed control, increased proportionally with heading error, enabling the robot to slow down when misaligned with the route. This behavior was consistent even when the robot was moved laterally off-route (Fig. 3a,b). Outdoors, these gradients were steeper (Fig. 3a,b,d and e), indicating a higher visual contrast with larger landmarks.

The model's ability to identify heading error accurately across training oscillation amplitudes up to 135° (Fig. 3i, see also Supplementary note 1 and Fig. S1) suggests that this parameter may not require further tuning below this threshold. However, larger oscillation amplitudes increased computation time, especially on the Raspberry Pi platform (0.4s for ±45°, Fig. 3i). Notably, the familiarity difference index (Fig. 3g) closely matched the spatial derivative of the maximum familiarity index, corresponding to the catchment area and turn rate amplitude observed in ants (Fig. 3h, Supplementary note 1, 2, Fig. S1 and S2 [43]).

This analysis helped establish the operational limits of our MB model, maintaining stable behavior within a lateral error (d) of 2 meters and an angular error (θ_e) within the learning oscillation amplitude, set here at 45°. For asymptotic stability (i.e., the system's ability to return to equilibrium), we assumed a proportional relationship between λ_{diff} and θ_e, supported by the Pearson correlation coefficient being close to 1 (Fig. 3i) and expressed as $K_{diff} \cdot \lambda_{diff} = -\theta_e$, where K_{diff} is a tuned negative gain. Integrating this relationship into the robot's motion equations, we applied a Lyapunov function for stability analysis. Results confirmed that the system converged to equilibrium points at $d^e = 0$ and $\theta_e^e = 0$, effectively correcting small deviations and enabling the robot to remain aligned with the learned route. The full derivation of these equations and Lyapunov stability proof are provided in the Methods (section 6) and Supplementary note 3,4 and Fig. S3.

Route-following: robustness to visual changes

The proposed self-supervised approach for route learning was validated through a series of indoor and outdoor route-following tasks in fully autonomous mode, with

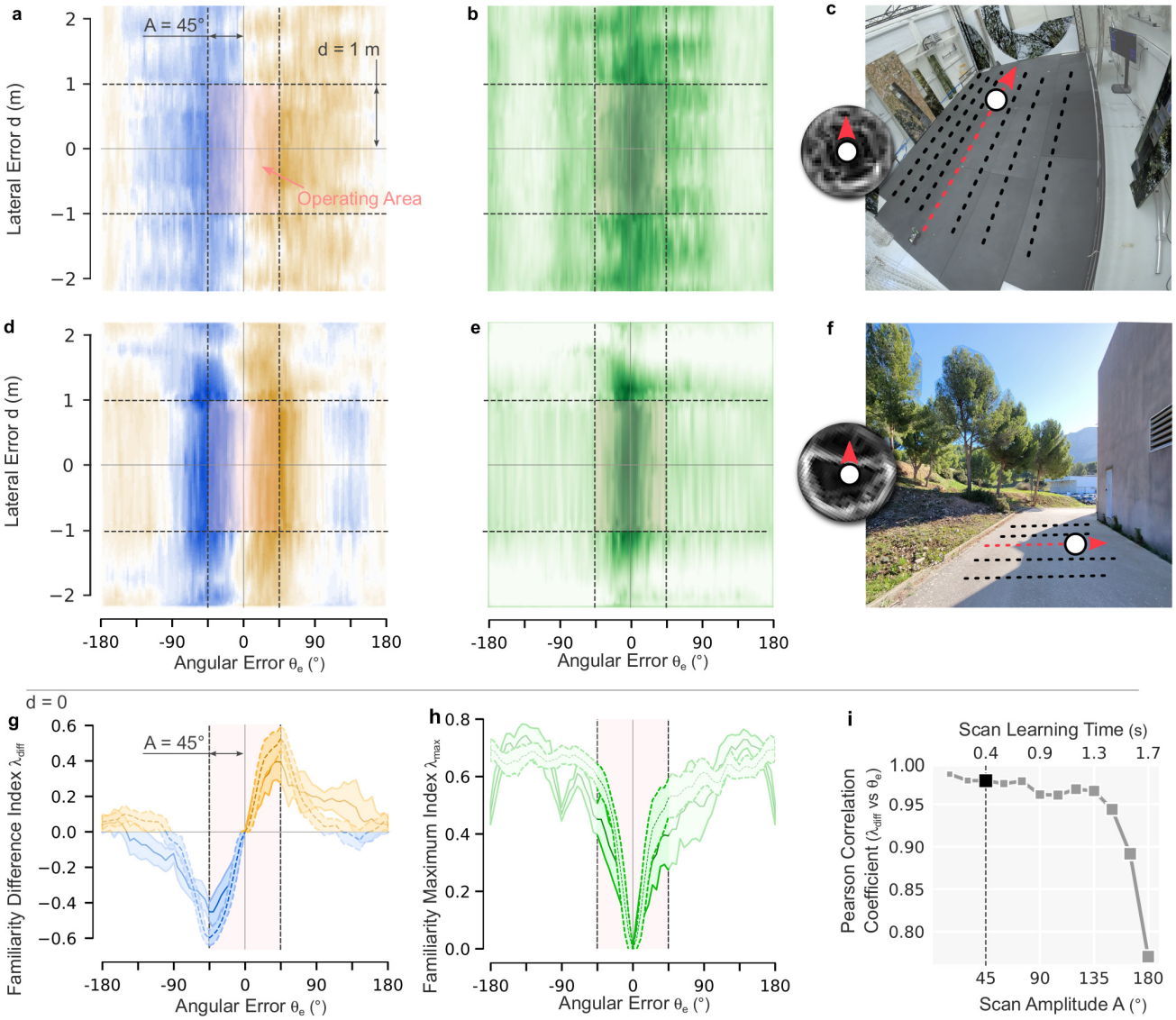

Fig. 3 Offline familiarity mapping for learning of indoor and outdoor routes. This figure illustrates the differentiation and maximum familiarity of route Mushroom Body Output Neurons (MBONs) during offline analysis of panoramic images and positional data from indoor (Mediterranean Flight Arena) and outdoor (Luminy Campus, Marseille, France) environments. The mapping was performed using an oscillation amplitude A of 45°. **a,d** Familiarity difference index (λ_{diff}) and **b,e** familiarity maximum index (λ_{max}) are mapped in the route's frame of reference, showing variations with both lateral and angular errors (d and θ_e). The defined operating area is highlighted in pink. **c** Overview of the indoor (top) and **f** outdoor (bottom) environments with the learned route highlighted in red. **g** Cross-sectional view of the familiarity difference index (λ_{diff}) and **h** familiarity maximum index (λ_{max}) against the angular error (θ_e) when the lateral error (d) is null. Plotted for indoor (solid line) and outdoor (dotted line) conditions. **i** Pearson correlation coefficient illustrating the linear relationship between familiarity difference index (λ_{diff}) and angular error (θ_e) as a function of oscillation amplitude A. This evolution of the correlation coefficient also illustrates the learning time required for a single oscillation cycle for each image captured on board the robot.

only two MBONs. After a first outbound route with online learning, where images were captured continuously to update synaptic weights in real-time, the robot demonstrated robust route-following in various configurations (Figs. 4 and 5). First, the Antcar robot successfully navigated convex and concave routes in a cluttered indoor environment of approximately 8 meters (median lateral error ±median absolute deviation (MAD) = 0.21 ± 0.09 m, angular error ±MAD = 3.4 ± 6.2°, Fig. 4a,g and Fig. 7a). Moreover, the robot showed resilience in a kidnapped robot scenario, realigning with the learned route after being displaced (lateral error ±MAD = 0.26 ± 0.14 m, angular error ±MAD = 6.45 ± 4.19°, Fig. 4b and Fig. 7a). Only one crash occurred when the robot exceeded theoretical angular limits (see Supplementary Fig. S5).

Further tests assessed the robot's adaptability to high and low light conditions (Figs. 4c,h and Figs. 4d,i). Despite a single learning trial under standard lighting (815 Lux), the robot accurately followed its route in high (1,340 Lux) and low (81 Lux) lighting, with similar lateral and angular errors across tests (Fig. 7). This indicates that the MB-based control system is robust to significant changes in illumination.

In dynamic conditions with pedestrians and camera occlusions (Figs. 4e,f), the robot maintained reliable route-following when encountering pedestrians (lateral error ±MAD = 0.27 ± 0.15 m, angular error ±MAD = 4 ± 2.8°, Fig. 4e and Fig. 7a) and with dynamic occlusions (lateral error ±MAD = 0.22 ± 0.13 m, angular error ±MAD = 4.7 ± 3.3°, Fig. 4f and Fig. 7a). The presence of pedestrians and occlusions was reflected by the

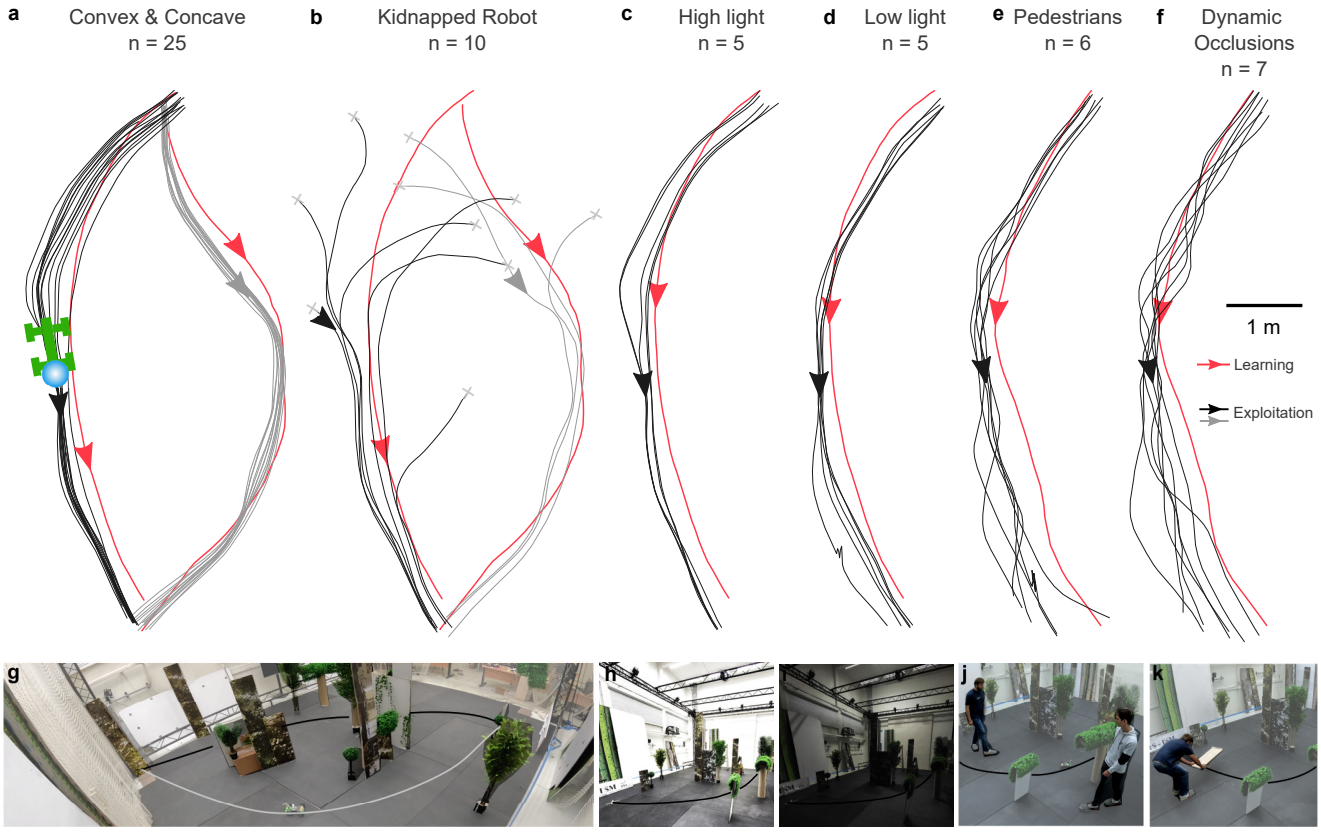

Fig. 4 Real world experiments of indoor route following in different conditions. The learned route in red is approximately 8m long. These experiments used two route MBONs. Environmental configurations and specific familiarity data are provided in the Supplementary Fig. S4 and video. **From a to f**, Route following results using the proposed self-supervised one-shot learning approach in different environmental conditions. **From g to k**, The visual environments in which the robot evolved during the experiments.

loss of maximum familiarity and led to speed reductions and increased emerging oscillatory motion (15% slower than in the previous experiments, Figs. 4e,f and supplementary video), which was also observed near obstacles. These results underscore the system's resilience under challenging conditions.

Outdoor experiments demonstrated the model's ability to maintain stable performance even over a long, 53-meter route and under altered environmental conditions. A route was learned and accurately recapitulated on a sunny day (lateral error ±MAD = 0.39 ± 0.13 m, angular error ±MAD = 5.8 ± 2.8°, Fig. 5a & 7a) and then retested the following day with parked cars removed (lateral error ±MAD = 1.3 ± 0.5 m, angular error ±MAD = 6.2 ± 3.2°, Fig. 5b & 7a). While the robot's error margins were slightly broader on the second day, it remained well within acceptable limits over the entire route. To test Antcar's maximum speed, a higher speed gain was applied during the second test (Fig. 5b), resulting in a cruising speed of 1.5 m/s compared to 1 m/s on the first day (see Supplementary Information note 5, Fig. S4 and Table S7).

Homing: homeward route and stop

Building on the validated route-following strategy, further tests refined the robot's behavior, focusing on ant-like homing. Homing, by definition, is the ability to return to a specific location after displacement. To test this, we evaluated the robot's ability to follow a 50 m outdoor route in reverse, stopping at a designated Nest area (point N in Fig. 6a). During learning, a 180° shift in the visual oscillation pattern simulated the "turn back and look" behavior observed in ants and led to homeward route following.

The robot successfully followed the 50 m route in reverse under cloudy outdoor conditions (lateral error ±MAD = 0.9 ±0.5 m, angular error ±MAD = 6.3 ±4.2°, Fig. 6a and Fig. 7a). Although maximum familiarity was higher than in previous outdoor experiments (see Supplementary note 5, Fig. S4 and Table S7), overall accuracy remained stable and emerging oscillatory movements was demonstrated (see Supplementary Video).

To enable autonomous stopping at the Nest, a place-specific MBON was used to learn 'nest-views' at the starting point of the route. Subsequent 'recognition' in this MBON, based on a familiarity threshold, acted as a motivational cues to halt route-following behavior and reducing the robot's linear velocity. This mechanisms was sufficient for the robot to successfully reach and stop at the Nest area in 4 out of 5 trials, with a median stopping distance of 1.4 m (Fig. 6c, see also Supplementary Fig. S6b for detailed familiarities values over distance).

Shuttling: foodward and homeward routes

Reverse route-following is also commonly observed in ants and was successfully replicated on board Antcar. Homing ants can pull food items backward when it is too large to carry forward, maintaining body alignment with the outbound route learned forward, and

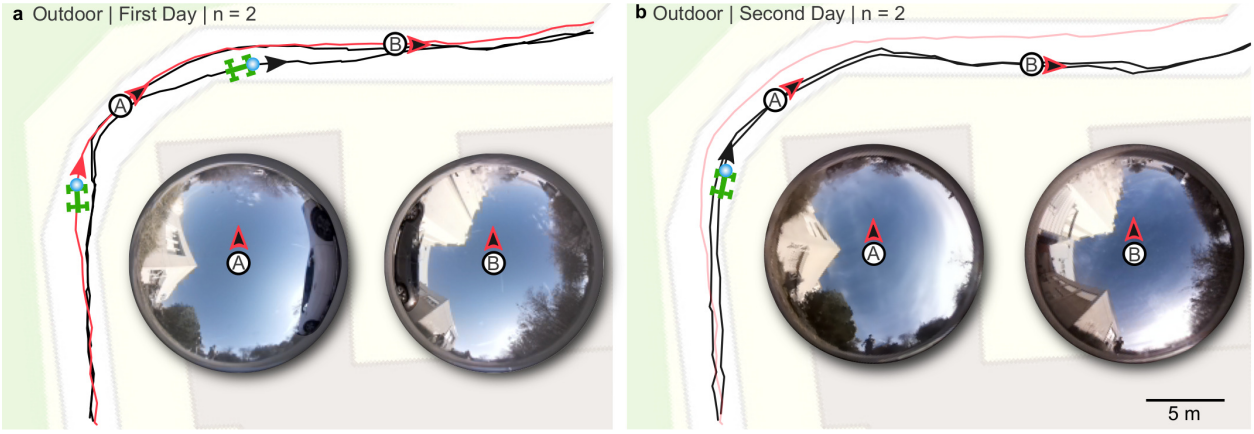

Fig. 5 Real word experiments of outdoor route-following with shared memories. a First day experiments, learning and autonomous route with several cars along the road. **b** Second day experiments, autonomous routes using the memories from day one in an altered environment (without cars).

using outbound memories with an opposite valance [50]. Shuttling tests show the robot's ability to switch movement direction and drive backward while maintaining alignment with the outbound route (Fig. 6b).

This foraging behavior was made possible by incorporating two additional place MBONs, which learned a series of panoramic views defining each endpoint of the route (Feeder and Nest). During shuttling, the model triggered a switch in motor gain polarity upon recognizing these panoramic views corresponding to the Feeder or Nest areas. In a cluttered indoor environment along a 6-meter learned route, the robot autonomously shuttled *to and fro* between the Feeder and the Nest, covering a total distance of 160 meters without interruption. Using a similar familiarity threshold on the two route-extremity MBONs, the robot detected the endpoints 22 times, achieving a median stopping distance of 0.31 m (Fig. 6d) (See Supplementary Fig. S6a for detailed familiarities values over distance).

This continuous shuttling revealed distinct differences in error profiles between forward and backward movement (Fig. 6b). During forward motion, the robot maintained stable control with minimal deviations (lateral error $\pm$MAD = 0.1 $\pm$ 0.03 m, angular error $\pm$MAD = 1.26 $\pm$ 0.83°, Fig. 6b). However, during backward motion, the traction-driven setup amplified steering effects, resulting in slightly larger deviations from both accuracy and precision, though overall performance remained acceptable (lateral error $\pm$MAD = 0.19 $\pm$ 0.08 m, angular error $\pm$MAD = 2.7 $\pm$ 2.1°, Fig. 6b & 7a). The increased 'motor' variability led to lower visual recognition signal and thus usefully affected speed, which decreased by 14% compared to forward motion (see Supplementary note 5, Fig. S4 and Table S7). Nonetheless, the robot consistently realigned with the correct path after such minor deviations. These results highlight the model's versatility across different driving dynamics, capability to implement inverted steering, and adaptability to variations in motor kinematics and propulsion.

Performance summary

Across all experiments, including both indoor and outdoor route-following, homing and shuttling tasks, the model demonstrated robust and stable navigation performance, completing 99 autonomous trajectories with a total of 1.3 km traveled. The theoretical limits of the system were validated, with convergence toward equilibrium points consistently achieved under various environmental conditions, even in the presence of noise (lateral error $\pm$MAD = 0.22 $\pm$0.10 m, angular error $\pm$MAD = 3.8 $\pm$2.4°, Fig. 7b). Lateral errors were within acceptable margins for both indoor and outdoor contexts, aligning within the standard widths of roads in France (5m) and typical indoor corridor (1.5m).

Additionally, statistical analysis showed no significant differences in the lateral or angular errors across the eleven test scenarios (Kruskal-Wallis test, $H = 1.20$ for lateral error, p value ≈ 1; $H = 0.97$ for angular error, p value ≈ 1), underscoring the system's reliability across diverse conditions (see Statistical Information). These results highlight the robustness and adaptability of the MB model in both structured and dynamic environments, confirming its potential applicability in a variety of navigation contexts.

Discussion

Our study presents a robust, embedded, and biologically inspired Mushroom Body (MB) model capable of long-distance navigation in the real world with minimal sensor acuity and computational resources. Using fewer than a thousand pixels, the Antcar robot successfully followed routes at speeds up to 1.5 m/s—approximately eight times its body length—achieving continuous online learning in just 20 ms per image, with exploitation times of 75 ms and an extrapolated memory footprint of only 0.3 Mo per kilometer. By integrating ant-inspired lateralized memory with self-supervised panoramic learning through oscillations, our model sustained high navigational accuracy across dynamic lighting, cluttered, and altered environments, with a positional accuracy of approximately 20 cm. Offline analysis confirmed the model's stability and alignment with defined limits, predicting robust real-time performance by reliably maintaining route alignment within learning oscillation bounds.

The angular error between the agent's head direction and the dynamic local route orientation (defined

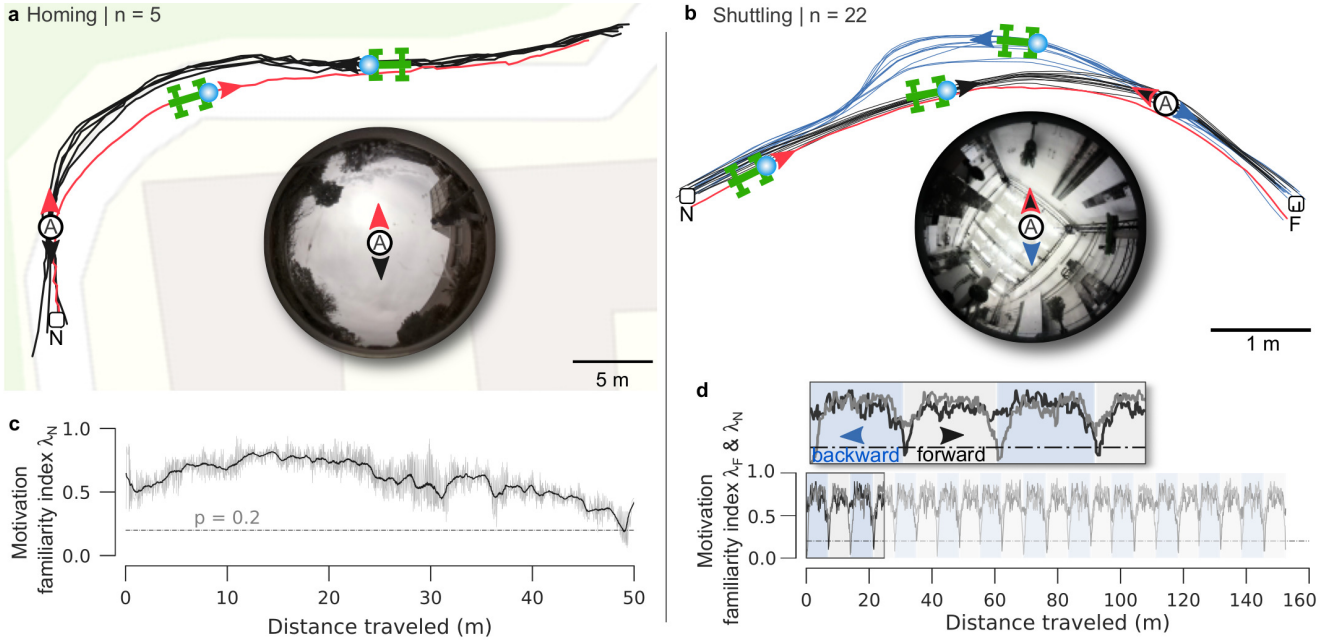

Fig. 6 Real word experiments of outdoor homing and indoor shuttling. a Homing experiments using two route MBONs and one motivation MBON for a 53m L-shaped route, in an outdoor cloudy environment. Autonomous route headed in the opposite direction. **b** Familiarity nest index (λ_N) over traveled distance with the fixed stopping condition ($p = 0.2$). **c** Shuttling experiments using two route MBONs and two place MBONs in an indoor environment with artificial visual cues. Autonomous routes swing back (blue) and forth (black). **d** Familiarity nest (λ_N) and feeder (λ_F) index over the traveled distance, zoomed in to illustrate backward and forward movement.

in the Methods as the Frenet frame [52]) emerged as both a challenge during exploitation—where the system minimizes this error—and a cue during learning, where the categorization process depends on its polarity. Our model demonstrated homing behavior using either a 180° shift in visual oscillation or by inverting motor gains, thus enabling forward and backward movements with only a single foodward learning route. Additionally, visual place memories stored in supplementary MBONs, paired with a motivational control system, allowed the robot to recognize route endpoints and modulate motor gain, halting movement or reverseing foraging motivation. With a single learning pass in one direction, the agent could follow the route forward, backward, and in reverse, controlled by oscillation parameters and motivational cues. Only motivational rules required adjustment to switch between route following, homing, and shuttling, underscoring the model's flexibility.

Our results surpass earlier ant-inspired familiarity-only models robots, which were generally limited to short indoor routes, slower linear speed (stop and scan), and lower efficiency [19–23]. Our model also markedly outperforms state-of-the-art visual teach-and-repeat methods, which report memory footprints of 3 Mo per kilometer and processing times around 400 ms [13]. Our model also achieves competitive results against teach-and-repeat systems incorporating odometry [14, 15].

This lateralized MB model distinguishes itself through reduced time and space complexity for route direction processing compared to perfect memory, snapshot, and visual compass approaches [43]. Whereas time and space complexity increase with the number of images in perfect memory or snapshot models, our MB model maintains constant space complexity, relying only on the synaptic matrix size KCtoMBON. Additionally, in contrast to visual compass approaches, where computational complexity scales with in-silico scan range and resolution during exploitation ($\mathcal{O}(n)$), our MB model maintains a constant factor ($\mathcal{O}(1)$) since in-silico scanning is only required during learning. For instance, while a visual compass scanning a ±45° range at 1° resolution requires 90 comparisons per image, our model requires only two comparisons, eliminating the need for angular scanning in exploitation. Notably, our model produced commands five times faster than the visual compass approach on the same robot platform [21].

Our contribution also aligns well with current biological observations, particularly highlighting the effectiveness of latent learning [53], where continuous learning bypass the need to control "when to learn" [31, 44]. The opposed event-triggered and snapshot-based learning models producing place learning [15, 54] where used here only to recognise place of interests such as the nest and the feeder to switch motivation, but were not engaged for route guidance. Also, our MB model prioritized body orientation within the local frame rather than divided the visual field [22, 46], aligning with biological observations in ants with unilateral visual impairment, showing that these insects store and recognise fudnamentally binocular views [47]. Interestingly, the linear relationship observed between familiarity measures (and thus motor output) and angular error during exploitation closely mirrors experimental findings in ants [43]. This relationship enabled us to demonstrate the asymptotical stability of the system within a defined domain, ensuring the consistent and predictable behavior essential for a robotic navigation model [55].

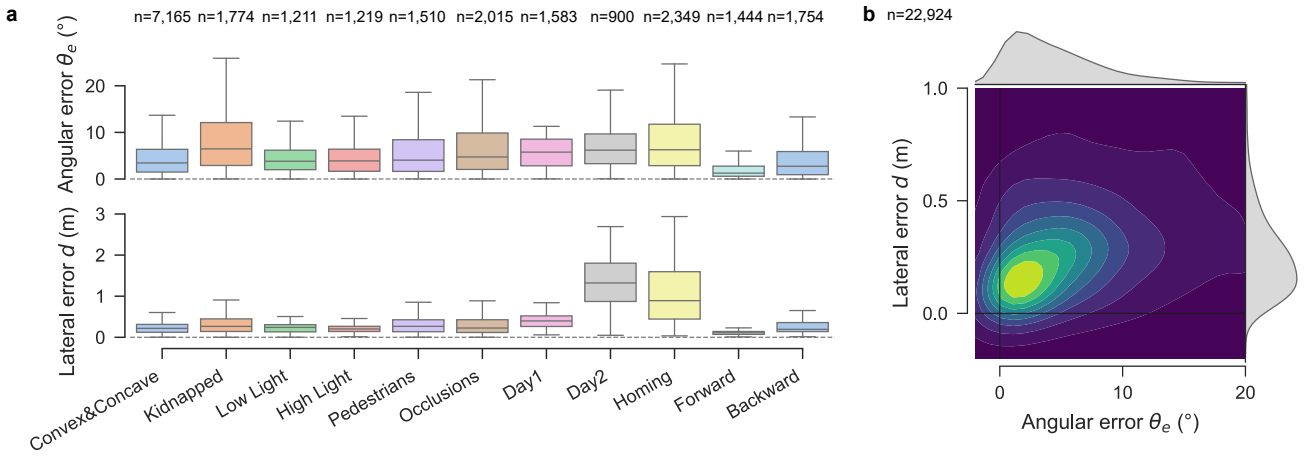

Fig. 7 Performance during route following overview a Detailed errors for each experiment. **b** Weighted bi-variate distribution for lateral (d) and angular errors (θ_e) across 11 different experimental configurations.

Furthermore, oscillatory learning behavior mirrors ant behavior, where initial routes involve slow, rotational movements, transitioning to direct paths on subsequent journeys [39]. These oscillations typically fall within ±100°, with peaks around ±45° in unfamiliar terrain [40, 42]. The robot's ability to slow down and produce emerging mechanical scanning upon entering unfamiliar areas (see Supplementary Video) are consistent with such naturalistic behaviors. Finally, Antcar's homing capability was maintained even when navigating backward, closely mirroring ant behavior while dragging food [48–50, 56]. Overall, our attemt to integrate multiple MBONs, oscillations, "turn back and look" behavior, and motivational control mechanisms echoes insect mechanisms [2, 57], and the resulting expression when implemented in the robot echoes insect behaviours.

This study addresses several core needs identified in research on embodied neuromorphic intelligence [6, 8], such as robustness to visual changes, adaptability to real-world environments, and support for extended route learning. Our algorithm's efficiency allows computational power for additional tasks, making it valuable in GPS-compromised or SLAM-disrupted scenarios (SLAM stands for Simultaneous Localization And Mapping). The robot's low-resolution, wide-angle vision proves resilient against moving objects that often disrupt SLAM. Our model is well-suited for dynamic environments or situations where odometry (e.g., visual, inertial, step-counting, or wheel-rotation) is unreliable.

Interestingly, the semi-random encoding process, specifically the PNtoKC synaptic projections, introduces a "fail-secure" memory-sharing mechanism. If synaptic weights for encoding differ, memory sharing becomes inaccessible, an advantageous feature for swarm robotics or cross-robot memory sharing.

Future research could enhance this approach. Transitioning this model to a spiking neural network on neuromorphic hardware could further enhance computational efficiency and biological fidelity [11]. Additionally, incorporating obstacle avoidance [58], would improve performance in dynamic environments.

In addition, a reduction of the visual field could correspond to more general cases, rendering in silico scanning impossible. In such scenarios, it would be necessary to estimate the angular error between the road frame and the agent. This could be achieved using a local angular path integration system (or odometry) during learning. As demonstrated by Collett et al. [59], showing that ants could utilize route segment odometry for navigation.

Our approach does not cover beeline homing post-foraging or search behaviors near points of interest, although these could be added by adding path integration mechanisms [60] or using the current visual mechanism but adding "learning walk" behaviors around place of interest [44]. Additionally, fixed neural parameters across all experiments suggest an opportunity for further exploration by adjusting Kenyon Cell numbers or connectivity, or testing different MB learning mechanisms [61].Expanding the number of MBONs, akin to the 34 in Drosophila [37], could enable more complex motivational states, multi-branch memory storage [53], and broader navigational abilities [62].

Overall, inspired by the neuroethology of ants, our MB model provides an effective bridge between theoretical insights and practical applications in insect-inspired autonomous robotic navigation. This egocentric model confirms the neuromorphic architecture's promise for autonomous systems, suggesting a scalable solution for both robotics and biological research applications.

Methods

This section describes the methodology used in the present study, focusing on the Encoding, Learning, and Exploitation processes of the proposed MB model (Figs. 2b-d). We also provide details on the hardware setup, control architecture, and stability analysis (See Supplementary Fig. S7 for the detailed route following neural network).

Image Encoding

Inspired by the visual system of ants [63], the model encoded real-world images into sparse, binary neural representations to efficiently handle visual input.

The encoding function (Fig. 2b) processed panoramic images from a camera with a 220° vertical and 360° horizontal field of view. This wide field of view enabled the camera to capture from slightly below the horizon to nearly directly below itself. To enhance natural contrast, the green channel of each image was selected [63], followed by Gaussian smoothing ($\sigma = 3$ pixels) to reduce noise. The image was then downsampled to an ultra-low-resolution 32×32 pixel thumbnail (0.145 pixel per degree), approximating the visual resolution of ants at 7.1° between adjacent photoreceptors.

Next, a Sobel filter extracted edges, mimicking lateral inhibition as seen in insect optical lobes [64]. These processed images were flattened into 800 Visual Projection Neurons (PNs), comparable to the number of ommatidia in ants. The PNs were further expanded into Kenyon Cells (KCs) using a fixed, sparse pseudo-random synaptic matrix (PNtoKC). Each KC received input from four PNs, enhancing the visual encoding's discriminative power within the Mushroom Body (MB) [65], forming an Excitatory Post Synaptic Projection (EP) vector of size u.

The EP vector size was set to $u = 15,000$ for the route MBONs ($MBON_R$ and $MBON_L$), while for place-specific MBONs ($MBON_N$ and $MBON_F$), which required fewer images, u was set to 5,000. A κ-Winner-Take-All (WTA) mechanism was applied to capture the highest contrasts, creating a high-dimensional, sparsified binary vector. This vector, referred to as the Action Potential (AP), consequently activated only 1% of KCs ($\kappa = 0.01$), giving $\overline{u} = u * \kappa$ active neurons. This final binary representation served as the encoded visual input.

All parameters were predefined by literature and experimental tests, but not further optimized.

Routes and places learning

The learning process is governed by synaptic depression through anti-Hebbian learning.

$$KCtoMBON_i = \begin{cases} 0, & \text{if } AP_i = 1 \\ KCtoMBON_i, & \text{otherwise} \end{cases} \quad (1)$$

For each MBONs, their synaptic weight matrix ($KCtoMBON$) dynamically adjusted their weight based on input from the AP layer described in equation 1 and from the mimicked dopaminergic feedback. Here, $_i$ represents the i^{th} neuron in the specified vector, with $KCtoMBON_i$ and AP_i in $\{0, 1\}$.

The simulated oscillatory movements during learning were obtained by rotating each captured image in steps, creating a sweep of rotations (θ_c) described by the following function:

$$\theta_c(n) = A \cdot \sin(n \cdot \Delta\theta + \phi) \quad \text{for } n = 0, 1, 2, \ldots, \frac{2A}{\Delta\theta} \quad (2)$$

where A represents the oscillation amplitude, $\Delta\theta$ the step size, and ϕ the phase shift. The step size was fixed at $\Delta\theta = 5°$, with $A = 45°$ for route MBONs and $A = 30°$ for place MBONs. The phase shift was $\phi = 180°$ only for the homing task (Fig. 6).

For route learning, the model assumed the robot perfectly aligned to the route being learned. The body rotation was estimated as $\hat{\theta}_e = \theta_e + \theta_c$, where therefore $\theta_e = 0$ during learning. The encoded binary image was categorized based on the polarity of $\hat{\theta}_e$, such that:

$$\begin{cases} Learn(AP, KCtoMBON_R), & \text{if } \hat{\theta}_e \leq 0 \\ Learn(AP, KCtoMBON_L), & \text{if } \hat{\theta}_e \geq 0 \end{cases} \quad (3)$$

Here, the function $Learn()$ follows equation 1. Synaptic weights (KCtoMBON) were stored in CSR format, achieving significant data compression to 148 kilobits independently of the route length, reducing memory requirements by 99.97% from cumulative image storage. This self-supervised model continuously learned visual input at high throughput without memory overload, as only novel views (i.e., newly recruited KCs) modulated synapses. Several panoramic views were learned to define the start and finish areas in their respective MBONs, serving as motivational cues.

Exploitation process and control architecture

During exploitation, the model calculated familiarity scores (λ) by comparing the current input (AP) with each MBON's synaptic weight matrix ($KCtoMBON$):

$$\lambda = \frac{1}{\overline{u}} \sum_{i=1}^{u} AP_i \cdot KCtoMBON_i \quad (4)$$

This familiarity score, ranging from 0 (unfamiliar) to 1 (familiar), was used to assess route alignment. The lateralized difference in familiarities between the left and right MBONs ($\lambda_{diff} = \lambda_L - \lambda_R$), which indicates whether the current view is more oriented to the left or right of the route, guided the robot's steering angle (φ). Meanwhile, the maximum familiarity ($\lambda_{max} = \max(\lambda_L, \lambda_R)$), representing how familiar the current view is, modulated its speed (v).

Thus, the control input U was defined as:

$$U = \begin{bmatrix} v \\ \varphi \end{bmatrix} = \begin{bmatrix} M \cdot K_v \cdot \text{sat}(1 - \lambda_{max}) \\ M \cdot K_\varphi \cdot \lambda_{diff} \end{bmatrix} \quad (1)$$

Here, K_v and K_φ are proportional gains that control linear and angular velocities, while the saturation function ($sat()$) establishes a minimum throttle level, ensuring minimum speed even at low familiarity levels. The motivational state (M) regulated transitions between behaviors based on a familiarity thresholds within place-specific MBONs. During route following, M was consistently set to 1. In homing experiments, where the objective was to stop at the nest, M initially started at 1 and switched to 0 once the familiarity of the nest-specific MBON (λ_N) fell below a fixed threshold ($p = 0.2$), signaling arrival at the nest. For shuttling tasks, M alternated between values of 1 and -1 as the

robot reached each route extremity, driven by a familiarity thresholds of the two place-specific MBONs (λ_N and λ_F).

Theoretical analysis of the robot stability

Stability in mobile agents, biological or robotic, is essential for reliable, predictable behavior. In control theory, an agent's motion is generally modeled as $\dot{x} = f(x, U)$, where x is the state vector (e.g., position or velocity), U is the control input, and f describes system dynamics. A desired equilibrium point x_e is achieved by defining a control input U_e such that $f(x_e, U_e) = 0$, allowing the system to maintain stability and return to equilibrium after disturbances. Stability is typically assessed using a Lyapunov function [55], which ensures the system converges to a stable state over time.

In contrast to conventional control approach, we applied a neuroethologically inspired control input derived from ant behavior, assessing stability via an a posteriori Lyapunov analysis. The robot's motion was modeled in a Frenet frame, a moving reference frame coincident with the nearest point on the route, to minimize lateral and angular errors, defined by $x = [d, \theta_e]$. Empirical data for stability assessment was collected in indoor and outdoor environments (paths of approximately 6 meters with 855 learned images each), providing distinct visual contexts (Figs. 2, 3). The robot's equations of motion from a global to the Frenet frame are [66]:

$$\begin{bmatrix} \dot{s} \\ \dot{d} \\ \dot{\theta}_e \end{bmatrix} = \begin{bmatrix} v\left(\cos\theta_e - \tan\varphi \sin\theta_e\right) \\ v\left(\sin\theta_e + \tan\varphi \cos\theta_e\right) \\ v\frac{\tan\varphi}{L} \end{bmatrix}, \qquad (5)$$

where s is the arc length along the route, d is the lateral error, and θ_e is the angular error.

This kinematic model, along with by empirical observations (Fig. 3), enabled us to establish an asymptotically stable domain for lateral and angular errors (d and θ_e), ensuring reliable route-following performance even with minor disturbances. The full theoretical stability proof and derivations of the model in the frenet frame are provided in the Supplementary note 3 and 4.

Antcar robot and ground truth system

The experiments were conducted using Antcar (Fig. 1 and Fig. 2a), a PiRacer AI-branded car-like robot. Antcar features four wheels, with two rear drive wheels powered by 37-520 DC motors (12V, 1:10 reduction rate) and a front steering mechanism controlled by an MG996R servomotor (9kg/cm torque, 4.8V). The robot's chassis measures 13×24×19.6 cm and is powered by three rechargeable 18650 batteries (2600mAh, 12.6V output). Antcar's primary sensor is a 220° Entaniya fisheye camera, mounted upward to capture panoramic images at $160 \times 160px \times 3$ resolution and 30 Hz, processed using OpenCV on a Raspberry Pi 4 Model B (Quad-core Cortex-A72, 1.8GHz, 4GB RAM), running Ubuntu 20.04. Note that there was no closed-loop control on the wheel rotation speed. Raspberry Pi manages real-time performance and controls the motors through a custom ROS architecture.

Real-time communication is facilitated by ROS Noetic, either via Wi-Fi (indoor) or a 4G dongle (outdoor). The robot can be controlled manually using a keyboard, joystick or with GPS waypoint, but in autonomous visual-only mode, it follows its own internal control law. Control inputs—steering angle (φ) and throttle (v) are processed using the PyGame library. Real-time data visualization and post-experiment monitoring are achieved via Foxglove.

Antcar has a maximum velocity of 1.5 m/s and a maximum steering angle of 1 rad, with a wheelbase of 0.15 m. The robot's configuration states $q = (x, y, \theta)$ were tracked using different systems. Indoor experiments utilized eighteen Vicon™ motion capture cameras, with infrared markers on Antcar providing precise tracking at 50 Hz with 1 mm accuracy. Outdoor experiments employed a GPS-RTK system with a SparkFun GPS-RTK Surveyor, providing 14 mm accuracy at 2 Hz (GPS-RTK stands for Global Positioning System - Real-Time Kinematic). Ground speed and angular speed were calculated through position differentiation. The base station used for GPS corrections was a Centipede LLENX station located at 24 km (Aeroport Marseille Provence) from the experiment site in Marseille. Note that the ground truth acquisition system was run on the Rapserry Pi along with the mushroom body model.

Lateral error was calculated by finding the nearest point on the learning route using the Euclidean distance, with the shortest distance representing the absolute lateral error. Angular error was defined as the absolute difference in heading between the nearest learning route point and the current position. The euclidean distance between the agent and the Nest or Feeder areas was calculated to estimate the distance when the robot switched behavior (i.e familiarity dropped below the threshold).

Statistical informations

The errors used for statistics were recorded at each command decision timing. Due to non-normality in error values (with outliers retained), Box-Cox transformations were applied to stabilize variance across experiments, reducing the impact of outliers caused by indoor obstacles that hid the robot from the motion capture system or by GPS-RTK inaccuracies outdoors. The groups was compared using the Kruskal-Wallis test [67], and median values are reported with median absolute deviation (MAD), as median ± MAD. The package python SciPy [68] was used for the statistics. The overall medians and bivariate distribution plots were weighted by the number of measurements per experiment for the Fig. 7.

Acknowledgments

The authors thank David Wood for revising the English in this study, Guillaume Caron for providing the camera reference, and Thomas Gaillard, Clément Serrasse, and Hamidou Diallo for their assistance during the robotic tests.

Declarations

- Funding: G.G. was supported by a doctoral fellowship grant from Aix Marseille University and the French Ministry of Defense (AID - Agence Innovation Défense, agreement #A01D22020549 ARM/DGA /AID). G.G., J.R.S. and F.R. were also supported by Aix Marseille University and the CNRS (Life Science, Information Science, and Engineering and Science & technology Institutes). The facilities for the experimental tests has been mainly provided by ROBOTEX 2.0 (Grants ROBOTEX ANR-10-EQPX-44-01 and TIRREX ANR-21-ESRE-0015).

- Conflict of interest: the authors declare no competing interests.
- Data availability: Upon publication
- Code availability: Upon publication
- Supplementary Video : https://youtu.be/Osu5Jyy6dF4
- Author contribution: G.G., A.W., J.R.S., and F.R. designed this research work; G.G, A.W., J.R.S., and F.R. got funding for this study; G.G. performed experiments, collected and visualized the data; G.G., A.W., J.R.S., and F.R. analyzed data; G.G. wrote the first full draft. All authors reviewed the results and approved the final version of the manuscript.

References

[1] Franceschini, N. Small Brains, Smart Machines: From Fly Vision to Robot Vision and Back Again. *Proceedings of the IEEE* **102**, 751–781 (2014).

[2] Webb, B. & Wystrach, A. Neural mechanisms of insect navigation. *Current Opinion in Insect Science* **15**, 27–39 (2016).

[3] Denuelle, A. & Srinivasan, M. V. *A sparse snapshot-based navigation strategy for UAS guidance in natural environments*, 3455–3462 (IEEE, 2016).

[4] Glick, P. E., Balaram, J. B., Davidson, M. R., Lyons, E. & Tolley, M. T. The role of low-cost robots in the future of spaceflight. *Science Robotics* **9**, eadl1995 (2024).

[5] Yang, G.-Z. *et al.* The grand challenges of *Science Robotics*. *Science Robotics* **3**, eaar7650 (2018).

[6] de Croon, G. C., Dupeyroux, J., Fuller, S. B. & Marshall, J. A. Insect-inspired ai for autonomous robots. *Science Robotics* **7**, eabl6334 (2022).

[7] Mangan, M. *et al.* A virtuous cycle between invertebrate and robotics research: Perspective on a decade of Living Machines research. *Bioinspiration & Biomimetics* **18**, 035005 (2023).

[8] Bartolozzi, C., Indiveri, G. & Donati, E. Embodied neuromorphic intelligence. *Nature Communications* **13**, 1024 (2022).

[9] Webb, B. Robots in invertebrate neuroscience. *Nature* **417**, 359–363 (2002).

[10] Franz, M. O. & Mallot, H. A. Biomimetic robot navigation. *Robotics and Autonomous Systems* (2000).

[11] Sandamirskaya, Y., Kaboli, M., Conradt, J. & Celikel, T. Neuromorphic computing hardware and neural architectures for robotics. *Science Robotics* **7**, eabl8419 (2022).

[12] Simon, M., Broughton, G., Rouček, T., Rozsypálek, Z. & Krajník, T. in *Performance Comparison of Visual Teach and Repeat Systems for Mobile Robots* (eds Mazal, J. *et al.*) *Modelling and Simulation for Autonomous Systems*, Vol. 13866 3–24 (Springer International Publishing, Cham, 2023).

[13] Stelzer, A., Vayugundla, M., Mair, E., Suppa, M. & Burgard, W. Towards efficient and scalable visual homing. *The International Journal of Robotics Research* **37**, 225–248 (2018).

[14] Nourizadeh, P., Milford, M. & Fischer, T. Teach and Repeat Navigation: A Robust Control Approach. *2024 IEEE International Conference on Robotics and Automation (ICRA)* 2909–2916 (2024).

[15] Van Dijk, T., De Wagter, C. & De Croon, G. C. H. E. Visual route following for tiny autonomous robots. *Science Robotics* **9**, eadk0310 (2024).

[16] Mangan, M. & Webb, B. Spontaneous formation of multiple routes in individual desert ants (Cataglyphis velox). *Behavioral Ecology* **23**, 944–954 (2012).

[17] Kohler, M. & Wehner, R. Idiosyncratic route-based memories in desert ants, Melophorus bagoti: How do they interact with path-integration vectors? *Neurobiology of Learning and Memory* **83**, 1–12 (2005).

[18] Wystrach, A., Schwarz, S., Schultheiss, P., Beugnon, G. & Cheng, K. Views, landmarks, and routes: how do desert ants negotiate an obstacle course? *Journal of Comparative Physiology A* **197**, 167–179 (2011).

[19] Kodzhabashev, A. & Mangan, M. Wilson, S. P., Verschure, P. F., Mura, A. & Prescott, T. J. (eds) *Route Following Without Scanning.* (eds Wilson, S. P., Verschure, P. F., Mura, A. & Prescott, T. J.) *Biomimetic and Biohybrid Systems*, Vol. 9222, 199–210 (Springer International Publishing, Cham, 2015).

[20] *Insect-Inspired Visual Navigation On-Board an Autonomous Robot: Real-World Routes Encoded in a Single Layer Network*, Vol. ALIFE 2019: The 2019 Conference on Artificial Life of *Artificial Life*

Conference Proceedings.

[21] Gattaux, G., Vimbert, R., Wystrach, A., Serres, J. R. & Ruffier, F. Antcar: Simple route following task with ants-inspired vision and neural model. Preprint at https://hal.science/hal-04060451v1 (2023).

[22] Lu, Y., Cen, J., Maroun, R. A. & Webb, B. Embodied visual route following by an insect-inspired robot. Preprint at https://www.researchsquare.com/article/rs-4222706/latest (2024).

[23] Jesusanmi, O. O. *et al.* Investigating visual navigation using spiking neural network models of the insect mushroom bodies. *Frontiers in Physiology* **15**, 1379977 (2024).

[24] Caron, G., Marchand, E. & Mouaddib, E. M. Photometric visual servoing for omnidirectional cameras. *Autonomous Robots* **35**, 177–193 (2013).

[25] Cartwright, B. A. & Collett, T. S. Landmark learning in bees: Experiments and models. *Journal of Comparative Physiology ? A* **151**, 521–543 (1983).

[26] Möller, R. & Vardy, A. Local visual homing by matched-filter descent in image distances. *Biological cybernetics* **95**, 413–430 (2006).

[27] Zeil, J., Hofmann, M. I. & Chahl, J. S. Catchment areas of panoramic snapshots in outdoor scenes. *Journal of the Optical Society of America A* **20**, 450 (2003).

[28] Wystrach, A., Cheng, K., Sosa, S. & Beugnon, G. Geometry, features, and panoramic views: ants in rectangular arenas. *Journal of Experimental Psychology: Animal Behavior Processes* **37**, 420 (2011).

[29] Gaffin, D. D. & Brayfield, B. P. Autonomous Visual Navigation of an Indoor Environment Using a Parsimonious, Insect Inspired Familiarity Algorithm. *PLOS ONE* **11**, e0153706 (2016).

[30] Philippides, A., Baddeley, B., Cheng, K. & Graham, P. How might ants use panoramic views for route navigation? *Journal of Experimental Biology* **214**, 445–451 (2011).

[31] Baddeley, B., Graham, P., Husbands, P. & Philippides, A. A Model of Ant Route Navigation Driven by Scene Familiarity. *PLoS Computational Biology* **8**, e1002336 (2012).

[32] Wystrach, A., Beugnon, G. & Cheng, K. Ants might use different view-matching strategies on and off the route. *Journal of Experimental Biology* **215**, 44–55 (2012).

[33] Linsker, R. Self-organization in a perceptual network. *Computer* **21**, 105–117 (1988).

[34] Wystrach, A., Mangan, M., Philippides, A. & Graham, P. Snapshots in ants? new interpretations of paradigmatic experiments. *Journal of Experimental Biology* **216**, 1766–1770 (2013).

[35] Heisenberg, M. Mushroom body memoir: From maps to models. *Nature Reviews Neuroscience* **4**, 266–275 (2003).

[36] Eichler, K. *et al.* The complete connectome of a learning and memory centre in an insect brain. *Nature* **548**, 175–182 (2017).

[37] Aso, Y. *et al.* Mushroom body output neurons encode valence and guide memory-based action selection in Drosophila. *eLife* **3**, e04580 (2014).

[38] Ardin, P., Peng, F., Mangan, M., Lagogiannis, K. & Webb, B. Using an Insect Mushroom Body Circuit to Encode Route Memory in Complex Natural Environments. *PLOS Computational Biology* **12**, e1004683 (2016).

[39] Haalck, L. *et al.* CATER: Combined Animal Tracking & Environment Reconstruction. *SCIENCE ADVANCES* (2023).

[40] Deeti, S., Cheng, K., Graham, P. & Wystrach, A. Scanning behaviour in ants: An interplay between random-rate processes and oscillators. *Journal of Comparative Physiology A* (2023).

[41] Wystrach, A., Philippides, A., Aurejac, A., Cheng, K. & Graham, P. Visual scanning behaviours and their role in the navigation of the australian desert ant melophorus bagoti. *Journal of Comparative Physiology A* **200**, 615–626 (2014).

[42] Clement, L., Schwarz, S. & Wystrach, A. An intrinsic oscillator underlies visual navigation in ants. *Current Biology* **33**, 411–422 (2023).

[43] Wystrach, A., Le Moël, F., Clement, L. & Schwarz, S. A lateralised design for the interaction of visual memories and heading representations in navigating ants. Preprint at https://www.biorxiv.org/content/10.1101/2020.08.13.249193v1 (2020).

[44] Wystrach, A. Neurons from pre-motor areas to the Mushroom bodies can orchestrate latent visual learning in navigating insects. Preprint at https://www.biorxiv.org/content/10.1101/2023.03.09.531867v1 (2023).

[45] Stürzl, W., Zeil, J., Boeddeker, N. & Hemmi, J. M. How Wasps Acquire and Use Views for Homing. *Current Biology* **26**, 470–482 (2016).

[46] Steinbeck, F. *et al.* Familiarity-taxis: A bilateral approach to view-based snapshot navigation. *Adaptive Behavior* 10597123231221312 (2024).

[47] Schwarz, S., Clement, L., Haalck, L., Risse, B. & Wystrach, A. Compensation to visual impairments

and behavioral plasticity in navigating ants. *Proceedings of the National Academy of Sciences* **121**, e2410908121 (2024).

[48] Ardin, P. B., Mangan, M. & Webb, B. Ant Homing Ability Is Not Diminished When Traveling Backwards. *Frontiers in Behavioral Neuroscience* **10** (2016).

[49] Pfeffer, S. E. & Wittlinger, M. How to find home backwards? Navigation during rearward homing of *Cataglyphis fortis* desert ants. *Journal of Experimental Biology* **219**, 2119–2126 (2016).

[50] Schwarz, S., Clement, L., Gkanias, E. & Wystrach, A. How do backward-walking ants (Cataglyphis velox) cope with navigational uncertainty? *Animal Behaviour* **164**, 133–142 (2020).

[51] Freas, C. A. & Spetch, M. L. Terrestrial cue learning and retention during the outbound and inbound foraging trip in the desert ant, cataglyphis velox. *Journal of Comparative Physiology A* **205**, 177–189 (2019).

[52] Frenet, F. Sur les courbes à double courbure. *Journal de mathématiques pures et appliquées* **17**, 437–447 (1852).

[53] Clement, L., Schwarz, S. & Wystrach, A. Latent learning without map-like representation of space in navigating ants. Preprint at https://www.biorxiv.org/content/10.1101/2024.08.29.610243v1 (2024).

[54] Möller, R. & Vardy, A. Local visual homing by matched-filter descent in image distances. *Biological Cybernetics* **95**, 413–430 (2006).

[55] Lyapunov, A. M. The general problem of the stability of motion. *International journal of control* **55**, 531–534 (1992).

[56] Webb, B. The internal maps of insects. *Journal of Experimental Biology* **222**, jeb188094 (2019).

[57] Aso, Y. *et al.* Mushroom body output neurons encode valence and guide memory-based action selection in drosophila. *elife* **3**, e04580 (2014).

[58] Schoepe, T. *et al.* Finding the gap: Neuromorphic motion-vision in dense environments. *Nature Communications* **15**, 817 (2024).

[59] Collett, T. S. & Collett, M. Route-segment odometry and its interactions with global path-integration. *Journal of Comparative Physiology A* **201**, 617–630 (2015).

[60] Stone, T. *et al.* An anatomically constrained model for path integration in the bee brain. *Current Biology* **27**, 3069–3085 (2017).

[61] Webb, B. Beyond prediction error: 25 years of modeling the associations formed in the insect mushroom body. *Learning & Memory* **31**, a053824 (2024).

[62] Sommer, S., Von Beeren, C. & Wehner, R. Multiroute memories in desert ants. *Proceedings of the National Academy of Sciences* **105**, 317–322 (2008).

[63] Aksoy, V. & Camlitepe, Y. Spectral sensitivities of ants–a review. *Animal Biology* **68**, 55–73 (2018).

[64] Wystrach, A., Dewar, A., Philippides, A. & Graham, P. How do field of view and resolution affect the information content of panoramic scenes for visual navigation? A computational investigation. *Journal of Comparative Physiology A* **202**, 87–95 (2016).

[65] Le Moël, F. & Wystrach, A. Vision is not olfaction: impact on the insect mushroom bodies connectivity. Preprint at https://www.biorxiv.org/content/10.1101/2024.08.31.610627v1 (2024).

[66] Applonie, R. & Jin, Y.-F. A novel steering control for car-like robots based on lyapunov stability. *2019 American Control Conference (ACC)* 2396–2401 (2019).

[67] Kruskal, W. H. & Wallis, W. A. Use of ranks in one-criterion variance analysis. *Journal of the American Statistical Association* **47**, 583–621 (1952).

[68] Virtanen, P. *et al.* Scipy 1.0: fundamental algorithms for scientific computing in python. *Nature methods* **17**, 261–272 (2020).

Supplementary Files

This is a list of supplementary files associated with this preprint. Click to download.

- ContinuousvisualnavigationSupplementaryInformation.pdf
- ContinuousvisualroutefollowingVF.mp4